# Convection-Radiation Interaction in Buoyancy-Induced Channel Flow

A. Moutsoglou* and Y. H. Wong†
*South Dakota State University, Brookings, South Dakota*

**The interaction of convection with radiation in buoyancy-induced flow in a channel is re-examined in order to better understand the effects of each flow configuration parameter. The analysis differs from that of Carpenter et al.[4] primarily in the definition of the dimensionless temperature. In this study, $\theta$ is based on the local temperature itself rather than the difference of the local and inlet temperature.[4] The present definition avoids the unnecessary complications introduced via the linearization of the radiative terms[4] that make the interpretation of the presented results rather awkward. The present analysis concentrates in demonstrating individually the effects of the rate of heat transfer, channel length, channel width, air inlet temperature, and surface emissivities on the temperature of the heated and adiabatic walls.**

## Nomenclature

$F$ = shape factor
$Gr_H^*$ = modified Grashof number, $g\beta q_{ref}H^4/\nu^2 k$
$g$ = gravitational acceleration
$H$ = channel width
$k$ = thermal conductivity
$L$ = channel length
$N$ = number of elemental surfaces
$P$ = dimensionless pressure
$Pr$ = Prandtl number
$p$ = pressure
$q$ = local heat flux from wall
$R$ = dimensionless radiation number, $\sigma q_{ref}^3 H^4/k^4$
$T$ = temperature
$U,V$ = dimensionless axial and transverse velocity components
$u,v$ = axial and transverse velocity components
$X,Y$ = dimensionless axial and transverse coordinates
$x,y$ = axial and transverse coordinates
$\alpha$ = thermal diffusivity
$\beta$ = coefficient of thermal expansion
$\epsilon$ = surface emissivity
$\theta$ = dimensionless temperature, $kT/q_{ref}H$
$\nu$ = kinematic viscosity
$\rho$ = density
$\sigma$ = Stefan-Boltzmann constant

## Introduction

THE interaction of radiation and convection in channels has been studied for forced convection flows with high surface temperatures[1,2] as well as for natural convection flows.[3,4] The radiation effects were explored by Sparrow et al.[3] for the case of a channel having one isothermal wall and one adiabatic wall. It was found that radiative transport between the heated and adiabatic walls increases the free convective heat transfer considerably. In related applications, such as the cooling of electronic equipment and fail-safe decay heat removal systems of breeder reactors, a more appropriate thermal boundary condition is the prescription of surface heat flux rather than temperature. This in effect complicates the computational handling of the radiation-convection interaction. Such a study was reported by Carpenter et al.[4] However, the choice of the dimensionless parameters used and the coarse linearization employed[4] makes the presented results very awkward and difficult to interpret. The significant relevance of the phenomenon in recent engineering applications coupled with the shortcomings of the available literature were the incentives for the reinvestigation of the problem.

Received May 2, 1988; revision received Aug. 5, 1988. 

*Associate Professor, Mechanical Engineering Department.
†Graduate Student, Mechanical Engineering Department.

## Analysis

The present study focuses on the interaction of radiation and convection for the natural flow of air in a heated two-dimensional channel. A schematic of the flow configuration and coordinate system is illustrated in Fig. 1. The channel consists of two vertical parallel plates of finite length $L$, spaced a distance $H$ apart. An asymmetric nonuniform heat flux is prescribed on the inside of each of the channel walls. The ambient quiescent air surrounding the channel is at a uniform temperature $T_\infty$. The surroundings enclosing the channel are considered to be large and at the uniform ambient temperature $T_\infty$. The air is assumed to be a radiatively nonparticipating medium. The dimensionless form of the governing system of equations for steady, two-dimensional laminar free convection flow in a vertical channel can be written as

$$\frac{\partial U}{\partial X} + \frac{\partial V}{\partial Y} = 0 \tag{1}$$

$$U\frac{\partial U}{\partial X} + V\frac{\partial U}{\partial Y} = -\frac{d\bar{P}}{dX} + \frac{\partial^2 U}{\partial Y^2} + \theta - \theta_\infty \tag{2}$$

$$U\frac{\partial V}{\partial X} + V\frac{\partial V}{\partial Y} = -\frac{\partial \bar{P}}{\partial Y} + \frac{\partial^2 V}{\partial Y^2} \tag{3}$$

$$U\frac{\partial \theta}{\partial X} + V\frac{\partial \theta}{\partial Y} = \frac{1}{Pr}\frac{\partial^2 \theta}{\partial Y^2} \tag{4}$$

where the Boussinesq approximation was used in modeling the buoyancy term. The dimensionless parameters appearing in

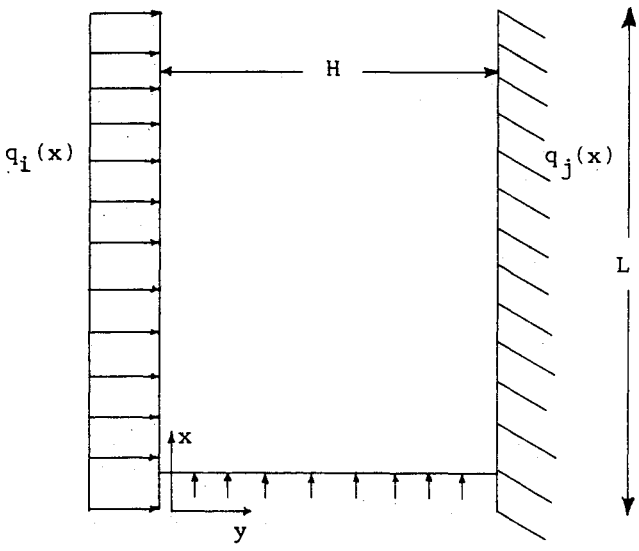


**Fig. 1 Flow schematic and coordinate system.**

Eqs. (1-4) are defined as follows:

$$X=\frac{x}{HGr_H^*}, \qquad Y=\frac{y}{H}, \qquad U=\frac{uH}{\nu Gr_H^*}, \qquad V=\frac{vH}{\nu}$$

$$\bar{P}=\frac{(\bar{p}-p_\infty)H^2}{\rho\nu^2 Gr_H^*}, \quad \hat{P}=\frac{\hat{p}H^2}{\rho\nu^2}, \quad \theta=\frac{kT}{q_{\text{ref}}H}, \quad \theta_\infty=\frac{kT_\infty}{q_{\text{ref}}H} \tag{5}$$

where $Gr_H^*$ is a modified Grashof number based on some reference heat flux, $q_{\text{ref}}$:

$$Gr_H^*=\frac{g\beta q_{\text{ref}}H^4}{\nu^2 k} \tag{6}$$

In formulating the governing conservation equations, the axial diffusion of momentum and heat was neglected. In addition, the longitudinal and lateral pressure gradients were decoupled by representing the local pressure $p(x,y)$ as the sum of a cross-sectional mean pressure $\bar{p}(x)$ that drives the axial flow, and a perturbation about the mean $\hat{p}(x,y)$ that drives the cross stream flow. Furthermore, the streamwise momentum equation reflects the local imbalance between the pressure within the channel and the corresponding hydrostatic pressure $p_\infty(x)$ outside.

The flow boundary conditions are given as

$$V=0 \text{ at } X=0,\ \bar{P}=0 \text{ at } X=0 \text{ and } X=L/HGr_H^*$$

$$U=V=0 \text{ at } Y=0 \text{ and } Y=1 \tag{7}$$

The thermal boundary conditions are specified as

$$\theta=\theta_\infty \text{ at } X=0 \tag{8}$$

$$\left.\frac{q_i}{q_{\text{ref}}}\right|_{Y=0}=-\left.\frac{\partial\theta_i}{\partial Y}\right|_{Y=0}+\epsilon_i R\theta_i^4|_{Y=0}$$
$$-\epsilon_i\sum_{m=1}^{N}F_{i-m}\left[\frac{(1-\epsilon_m)}{\epsilon_m}\left(\left.\frac{\partial\theta_m}{\partial Y}\right|_{Y=1}-\left.\frac{q_m}{q_{\text{ref}}}\right|_{Y=1}\right)\right.$$
$$\left.+R\theta_m^4|_{Y=1}\right]-\epsilon_i F_{i-\text{top}}R\theta_\infty^4-\epsilon_i F_{i-\text{bot}}R\theta_\infty^4$$
$$\text{at } Y=0 \text{ for } i=1,2\ldots,N \tag{9}$$

$$\left.\frac{q_j}{q_{\text{ref}}}\right|_{Y=1}=\left.\frac{\partial\theta_j}{\partial Y}\right|_{Y=1}+\epsilon_j R\theta_j^4|_{Y=1}$$
$$-\epsilon_j\sum_{n=1}^{N}F_{j-n}\left[\frac{(1-\epsilon_n)}{\epsilon_n}\left(-\left.\frac{\partial\theta_n}{\partial Y}\right|_{Y=0}-\left.\frac{q_n}{q_{\text{ref}}}\right|_{Y=0}\right)\right.$$
$$\left.+R\theta_n^4|_{Y=0}\right]-\epsilon_j F_{j-\text{top}}R\theta_\infty^4-\epsilon_j F_{j-\text{bot}}R\theta_\infty^4$$
$$\text{at } Y=1 \text{ for } j=1,2,\ldots,N \tag{10}$$

where $q$ denotes the prescribed elemental heat fluxes from the two walls, $N$ is the number of elemental surfaces on each wall, and $R$ is a radiation number defined from

$$R=\frac{\sigma q_{\text{ref}}^3 H^4}{k^4} \tag{11}$$

All surfaces were assumed to be gray and opaque, and the temperature of the surroundings was taken to be that of the quiescent ambient air $T_\infty$. The shape factors $F$, appearing in Eqs. (9) and (10), are evaluated systematically via a combination of Hottel's rule of crossed and uncrossed strings and the decomposition rule.

The number of dimensionless parameters in this study exceeds the corresponding number in the study of Carpenter et al.[4] by one. Specifically, the inlet temperature characterized by $\theta_\infty$ is not a direct required input in Ref. 4. This is because of the difference in the definition of the dimensionless temperature $\theta$, where it is based on the temperature difference $T-T_\infty$ in Ref. 4 rather than on $T$ itself, as seen from Eq. (5) in this study. The definition of $\theta$ based on $T-T_\infty$, which is the appropriate choice for pure convective flows, introduces complications in the linearization of the radiative terms. Thus, the linearization used in Ref. 4 results in requiring the estimation of an "average absolute surface-ambient temperature" defined in that study for the usability of the presented results. The value of such a dimensional temperature not only cannot be predetermined, but its approximation during the course of the solution from a dimensionless set of equations also seems to require the knowledge of the width and dimensional wall heat flux. With no such information available,[4] it is impossible for one to establish from the presented results the physical configuration that the authors[4] considered. In the present study, the choice of defining $\theta$ as in Eq. (5) not only accounts directly for the effect of the ambient temperature but also lacks any of the aforementioned ill effects due to the linearization, encountered in Ref. 4.

## Computational Procedure

Despite the parabolization of the governing differential equations described in the previous section, the system of equations is inherently elliptic via the boundary conditions. Whereas in pure free convection problems the ellipticity is caused because the inlet velocity is unknown while the pressure imbalance has to vanish at both the inlet and exit of the channel, in the combined convection-radiation problem the radiative terms in the thermal boundary conditions, Eqs. (9) and (10), are additionally elliptic in nature.

The streamwise momentum and energy equations [Eqs. (2) and (4)] were solved by using a control volume suggested by Patankar and Spalding[5] tailored for parabolic equations, while adopting the finite-difference procedure of Patankar[6] that employs the power law scheme for treating the convection-diffusion terms. A Newton-Raphson iterative method suggested by Raithby and Schneider[7] was used in computing the axial mean pressure gradient from the requirement of overall mass conservation at each streamwise location as the solution marched downstream. The transverse momentum equation (3) was solved at each cross stream plane using the Simpler algorithm

of Patankar,[6] with the control volumes staggered in the transverse direction. The transverse velocities were computed by imposing the continuity constraint. Each set of resultant algebraic equations was solved using the tridiagonal matrix algorithm of Thomas.

The computational scheme, in addition to invoking the standard local iterations at each streamwise location associated with the Patankar-Spalding and Patankar schemes, also required two global iterations on account of the two aforementioned causes of ellipticity. The unknown streamwise velocity at the inlet of the channel was assumed to be uniform, and its value was determined by the Newton-Raphson iteration scheme from the constraint that the mean pressure imbalance vanishes at the exit of the channel. A Gauss-Seidel iterative scheme was employed for handling the radiative terms in the thermal boundary conditions. Consequently, the procedure required the linearization of just the second term on the right-hand side of Eqs. (9) and (10). This was achieved by employing a Taylor series type of linearization,

$$\theta^4 \simeq \theta^{*4} + 4\theta^{*3}(\theta - \theta^*) \tag{12}$$

where $\theta^*$ is the current iterative value of the wall temperature. The remaining terms that involve temperatures raised to the fourth power were left as they are and were evaluated from their current iterative values.

Forty-three grid points were deployed in the transverse direction, while 21 rows of grid points ($N = 20$) were selected in the streamwise direction. Tests with 41 rows of grid points ($N = 40$) with 83 transverse grids in each row produced local wall temperature results that differed by less than 1.3% from those corresponding to the chosen mesh of 21 rows by 43 transverse grids, except for the first grid away from the inlet, where the deviation was as high as 3.5% for pure free convection and 2.3% for the combined convection-radiation case. Furthermore, an overall energy balance for the entire system using differences in bulk temperatures matched the prescribed wall heat flux for the pure free convection case within 1% for both grid configurations.

## Results

The primary concern of the current study is the assessment of the degree of contribution of radiation in altering the channel wall temperatures. Even though the analysis can be carried out for arbitrarily prescribed heat fluxes on each of the walls, the present results concentrate on the case studied in Ref. 4: a channel where one surface is heated uniformly while the other is kept insulated. With the reference heat flux chosen as the prescribed uniform flux, one symbolically has

$$\frac{q}{q_{\text{ref}}} = 1 \text{ at } Y = 0, \quad \frac{q}{q_{\text{ref}}} = 0 \quad \text{at } Y = 1 \tag{13}$$

for input into Eqs. (9) and (10), respectively.

With the left and right heat fluxes prescribed by Eq. (13), the four governing dimensionless parameters $L/H$, $Gr_H^*$, $\theta_\infty$, and $R$ are functions of only four physical dimensional variables, if one excludes the surface emissivities and the thermophysical properties of the fluid that are functions of some average temperature. These four variables are the channel length $L$, channel width $H$, fluid inlet temperature $T_\infty$, and the prescribed uniform heat flux on the heated left surface $q_{\text{ref}}$. There exists only one set of values for $L$, $H$, $T_\infty$, and $q_{\text{ref}}$ that corresponds to a set of $L/H$, $Gr_H^*$, $\theta_\infty$, and $R$, and vice versa; thus, the variation of one of the dimensionless parameters with the remaining three unchanged results in four different dimensional parameters. Consequently, a parametric study using dimensionless variables, as employed in Ref. 4, could not assess the individual effects of the channel length, channel width, wall heat flux, and ambient air temperature.

The parametric study here is thus concerned with the independent effects of each of these four dimensional variables on the heated and adiabatic wall temperatures. In estimating the corresponding dimensionless parameters for use in the solution algorithm, the thermophysical properties of the fluid are evaluated at the inlet temperature. In the figures that follow, only the dimensional physical variables with their appropriate units rather than the dimensionless parameters are chosen to be depicted. Whenever appropriate, the combined convection-radiation results are compared in the figures to those for pure free convection, which are obtained by replacing the thermal boundary conditions, Eqs. (9) and (10), by

$$\left.\frac{q_i}{q_{\text{ref}}}\right|_{Y=0} = -\left.\frac{\partial\theta_i}{\partial Y}\right|_{Y=0}, \qquad \left.\frac{q_j}{q_{\text{ref}}}\right|_{Y=1} = \left.\frac{\partial\theta_j}{\partial Y}\right|_{Y=1}$$

$$\text{for } i,j = 1,2,\ldots,N \tag{14}$$

in conjunction with Eq. (13).

The accuracy of the computational algorithm used was first tested by comparing the pure free convection results to the published numerical results of Aung et al.[8] for the case of asymmetric heating prescribed by Eq. (13). The predicted axial variation of the two surface temperatures is indistinguishable from those plotted in Fig. 7 of Ref. 8. A comparison was also made with the experimental results of Wirtz and Stutzman[9] that report data for natural convection between uniformly and

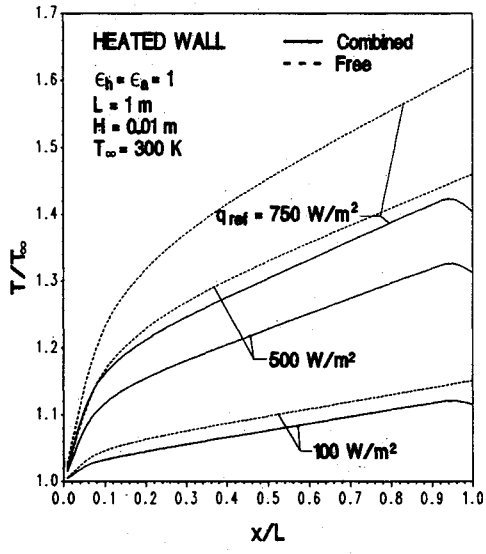


Fig. 2a Effect of rate of heat flux on the heated wall temperature.

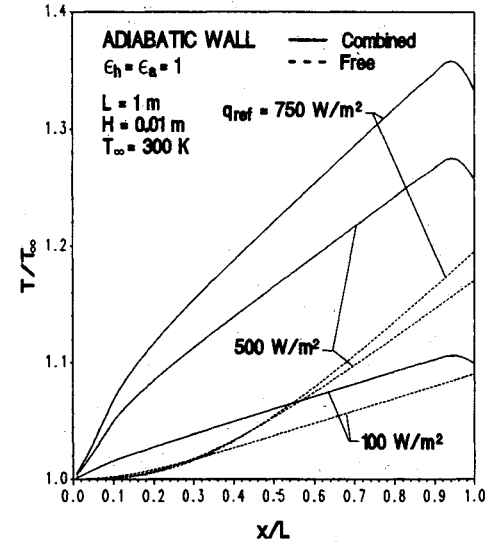


Fig. 2b Effect of rate of heat flux on the adiabatic wall temperature.

symmetrically heated parallel plates manufactured of stainless steel strips serpentined on phenolic printed circuit board. The combined convection-radiation algorithm with input data of $L = 0.3032$ m, $H = 0.0127$ m, and $q_{ref}$ of either 114.24 or 55.68 W/m$^2$ pertaining to the setup in Ref. 9, with assumed emissivities of 0.2 for both surfaces and $T_\infty = 300$ K, produced local surface wall temperatures for either flux case that could not be distinguished from the empirical data presented in Fig. 4 of Ref. 9. It is worthwhile to mention, though, that with the uniform symmetric heating and low emissivities, the radiation effects are negligible, and the excellent comparison does not serve as a strong assessment of the validity of the combined convection-radiation model. As the actual operating parameters of the data reported by Carpenter et al.[4] were not detailed, no such comparison was attempted herein.

The effects of the combined radiation-convection interaction on the channel wall temperatures are shown for three heat fluxes in Figs. 2a and 2b. Compared to free convection—dotted lines— the net radiation transfer from the heated to the adiabatic wall induces, as expected, a reduction in the temperature of the heated wall (Fig. 2a) while elevating the adiabatic wall temperature (Fig. 2b). While the maximum wall temperature for the pure free convection case always occurs at the exit of the channel, the maximum temperature for the combined interaction case occurs around $x/L = 0.9$ for both surfaces for the specified conditions in the two figures. It is the net radiation loss from the exit walls to the much colder surroundings that shifts the maximum temperature upstream in the channel and causes the hump seen in the graphs. The radiation-associated drop and elevation of the heated and adiabatic wall temperatures, respectively, are of the same order. For instance, the percent reduction of the heated wall temperature caused by radiation at midchannel, $x/L = 0.5$, is about 11.48% for $q_{ref} = 750$ W/m$^2$, 8.28% for 500 W/m$^2$, and 2% for 100 W/m$^2$. The corresponding elevations of the adiabatic wall temperature are, respectively, 13.66%, 9.64%, and 2.14%.

The transverse variation of the air temperature in the channel is plotted in Fig. 3 at streamwise locations near the inlet, midchannel, and exit. For pure free convection, the minimum temperature of the air always occurs at the adiabatic wall, $y/H = 1$. When radiation is accounted for, the minimum shifts very close to the center of the channel, $y/H = 0.5$, for all streamwise locations. The net radiation transfer from the heated to the adiabatic wall and the associated reduction of the heated wall temperature results in a reduction of the convective heat transfer to the fluid from the heated wall, as shown by the reduction of slope at $y/H = 0$. On the other hand, the respective elevation of the adiabatic wall temperature induces a convective flux at $y/H = 1$ that transfers the net radiation gain to the fluid via convection. The overall effect of the redistribution of the energy at each streamwise location is to bring the temperatures of the two walls closer together while tending to make the channel fluid isothermal. An interesting trend is observed at the adiabatic wall at the exit of the channel, where the temperature slope approaches zero for the combined mode. This is attributed to considerable radiative loss from the exit to the colder surroundings. Thus, under certain conditions, the fluid at the exit near the adiabatic wall may get hotter than the wall itself. This would eventually cause buoyancy-induced downwash velocities that invalidate the parabolicity of the conservation equations and result in the nonconvergence of the solution algorithm. For the specified conditions in Fig. 3, the modified Grashof number as defined by Eq. (6) is of the order of $Gr_H^* = 36{,}895$ which is still in the laminar regime.

To demonstrate the relative significance of the convection and radiation contribution to the total net heat flux, the streamwise variation of the net radiative flux leaving each surface is plotted, respectively, in Figs. 4a and 4b for the heated and adiabatic walls. It is noted that the first term on the right-hand side of Eqs. (9) and (10) represents the respective

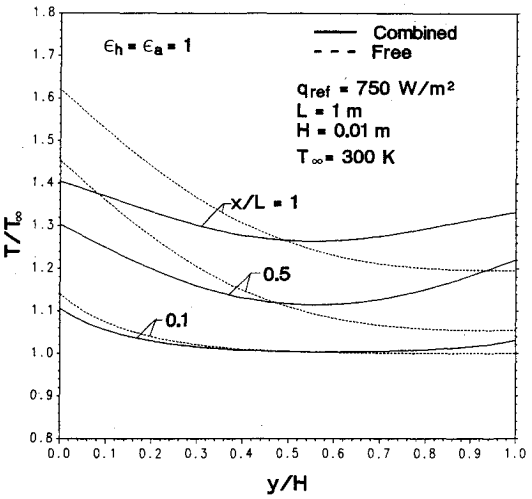


Fig. 3 Transverse temperature profiles of air.

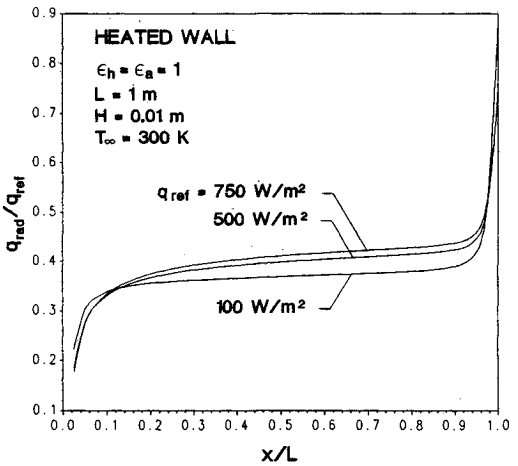


Fig. 4a Fraction of net radiative heat transfer from heated wall.

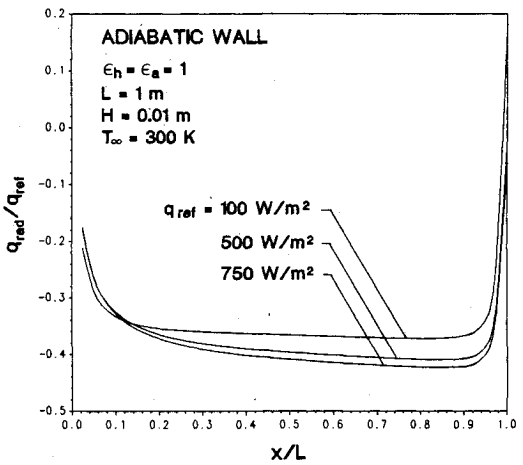


Fig. 4b Fraction of net radiative heat transfer from adiabatic wall.

net convective flux from the wall to the fluid, while the remaining terms on the right-hand side of each equation signify the net radiative flux leaving each surface. The convective and radiative heat fluxes are nondimensionalized with respect to the total net heat flux prescribed on the heated wall at each streamwise location. For the conditions specified by Eq. (13), the total net heat flux is represented by $q_{ref}$. Thus, the corresponding convective flux from the heated wall may be inferred by simply subtracting from unity the radiative distribution indicated in Fig. 4a. On the other hand, the respective con-

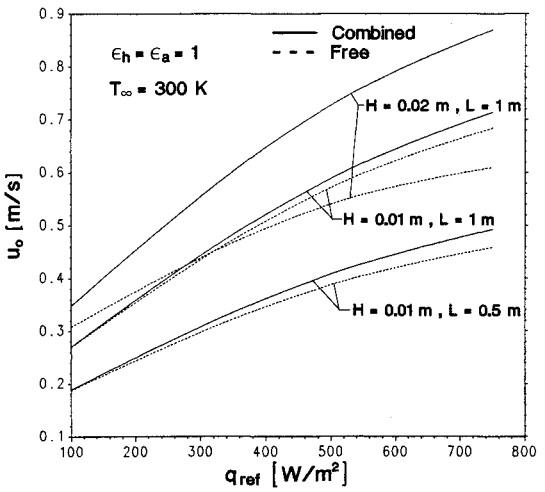


**Fig. 5 Effect of rate of heat flux on the average velocity of air.**

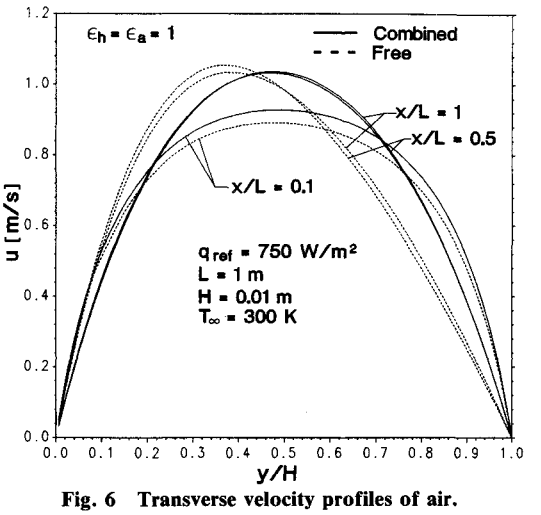


**Fig. 6 Transverse velocity profiles of air.**

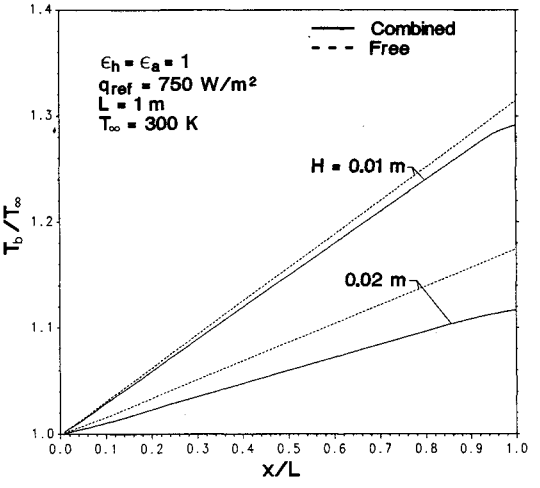


**Fig. 7 Axial variation of the bulk temperature of air.**

vective flux from the adiabatic wall is equal in magnitude and opposite in sign to the radiative distribution indicated in Fig. 4b.

As observed from Figs. 4a and 4b, the net radiative transfer remains constant throughout most of the channel, except near the inlet and primarily the exit. For the specified conditions, this constant ranges for both walls from 35–40% of the prescribed total flux as the flux varies from 100–750 W/m$^2$. An inspection of the two figures reveals that, in the majority of the channel excluding the exit, the net radiative transfer from the heated wall to the adiabatic wall is primarily between two directly opposing area segments as the net radiative loss of the heated wall is approximately equal to the net radiative gain of the adiabatic wall at each streamwise location. This is due to the smallness of the specified width of the channel, $H = 0.01$ m, that makes the shape factors between opposing segments close to unity. In addition, the adjacent surfaces that do participate in the radiation transfer are of comparable temperatures and thus do not contribute significantly to the net flux. This is not the case, however, near the channel exit, where the end segments are in thermal communication with the colder surroundings that are considered to be at the inlet air temperature. Consequently, the net radiative loss from the last wall segment of the heated wall increases sharply (Fig. 4a) as a significant portion of it goes to the surroundings, with an associated decrease in the magnitude of the net radiative gain of the adiabatic wall (Fig. 4b). As a result of this decrease, the net radiative heat flux from the last element on the adiabatic wall becomes positive for the case of $q_{ref} = 100$ W/m$^2$ and the configuration considered in Figs. 4a and 4b. This indicates that the adiabatic wall temperature at the exit is cooler than the adjacent fluid, even though no downwash velocities were noted.

The prediction of the net radiative flux for the very first and very last elements is strongly dependent on the number of axial points. This is due to the grid dependence of the shape factors, which is substantial for the two extreme elements at the inlet and exit of the channel exposed to the cooler surroundings. For this reason, the data in Figs. 4a and 4b are extracted from the results with a mesh of 41 × 83 grids. It is noted that the agreement for the net radiative heat flux between the results of 21 × 43 and those of 41 × 83 grids, excluding the first two grids away from the inlet and exit, is within 1% (0.2% at midchannel). Furthermore, the substantial deviations in the radiative flux of the inlet and exit elements produce significantly lesser deviations in local wall temperatures in the corresponding elements, as discussed in the previous section.

The effects of the radiation exchange on the average air velocity and subsequently on the airflow rate are depicted in Fig. 5, where the inlet velocity, assumed uniform a priori, is plotted as a function of the prescribed flux on the heated wall. The corresponding volumetric flow rate per unit depth of the channel can be easily deduced by multiplying the value of the inlet velocity by the appropriate channel width $H$ for the cases illustrated in Fig. 5. The net radiation transfer from the heated to the adiabatic wall and the subsequent convection transfer from the adiabatic wall to the fluid may cause significant increases in the average velocity and thus flow rate over those for pure free convection. As can be seen from the figure, these increases magnify with increasing channel width. Thus, for $q_{ref} = 750$ W/m$^2$, $L = 1$ m, and $H = 0.02$ m, the increase in the average velocity due to radiation is about 42%.

The transverse velocity profiles of the air in the channel for three streamwise locations corresponding to those in Fig. 3 are plotted in Fig. 6. As the net radiation transfer tends to bring the temperatures of the two walls closer at each streamwise location, the skewness of the free convection velocity profiles diminishes and a more parabolic type of shape prevails. This also seems to accelerate the hydrodynamic development of the velocity profiles, as can be attested from the figure.

The streamwise variation of the bulk temperature of the air is depicted in Fig. 7. Because of the net radiative losses to the cooler surroundings, the total energy transfer to the air is less than the corresponding case for free convection. This results in a decrease in the local value of the air bulk temperature when compared to that for free convection. The deviation increases as the channel exit is approached. As expected, the reduction in the bulk temperature caused by radiation becomes more significant with increasing channel width, as observed from the figure.

The effects of the length of the channel on the temperature of the heated and adiabatic walls are indicated in Figs. 8a and 8b, respectively. As larger average velocities persist with longer channels, an appropriate reduction in the temperature

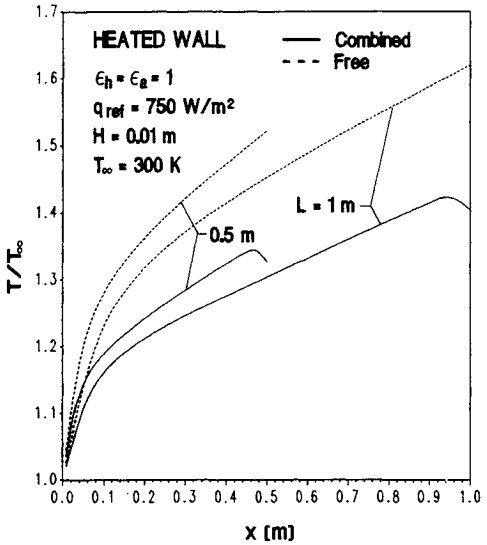


Fig. 8a Effect of channel length on heated wall temperature.

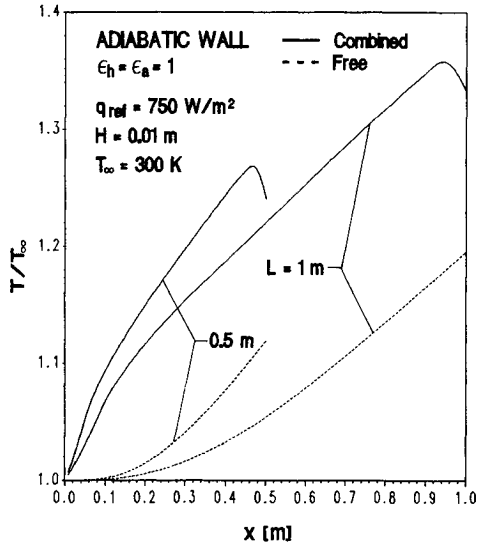


Fig. 8b Effect of channel length on adiabatic wall temperature.

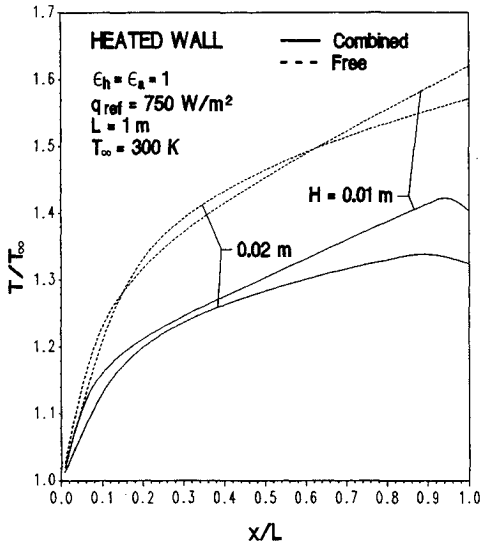


Fig. 9a Effect of channel width on heated wall temperature.

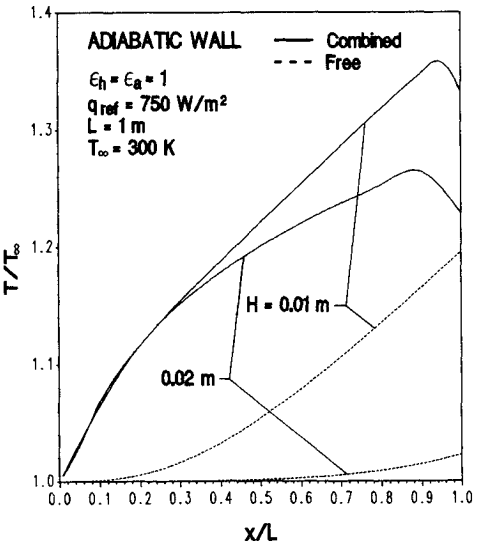


Fig. 9b Effect of channel width on adiabatic wall temperature.

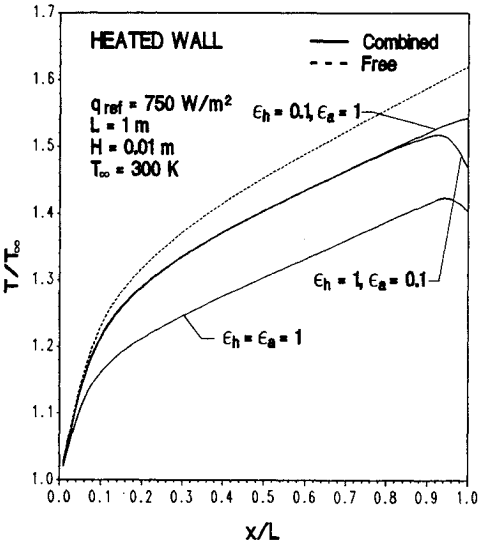


Fig. 10a Effect of surface emissivities on heated wall temperature.

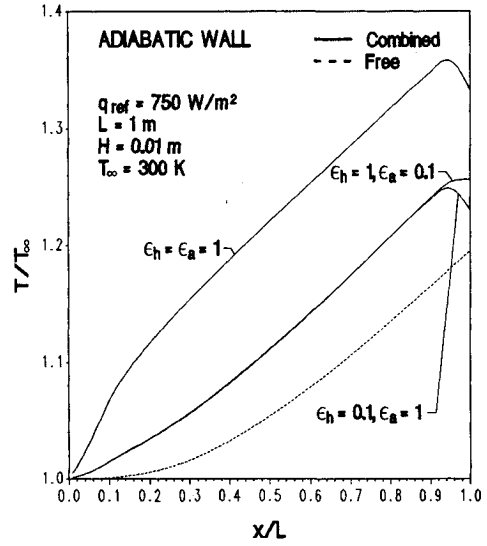


Fig. 10b Effect of surface emissivities on adiabatic wall temperature.

of the walls is experienced with length, as observed from the two figures. The magnitude of this reduction does not seem to be strongly dependent on the convection-radiation interaction for either wall.

Figures 9a and 9b portray the effects of the channel width on the heated and adiabatic wall temperatures, respectively. As seen from Fig. 9a, the variation of the heated wall temperature with the channel width becomes pronounced primarily in

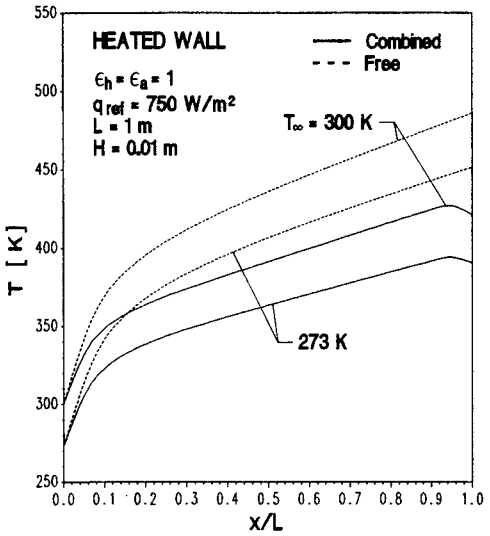


Fig. 11a Effect of inlet air temperature on heated wall temperature.

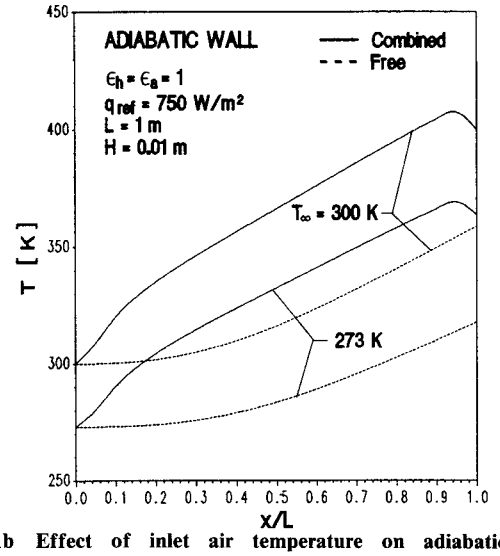


Fig. 11b Effect of inlet air temperature on adiabatic wall temperature.

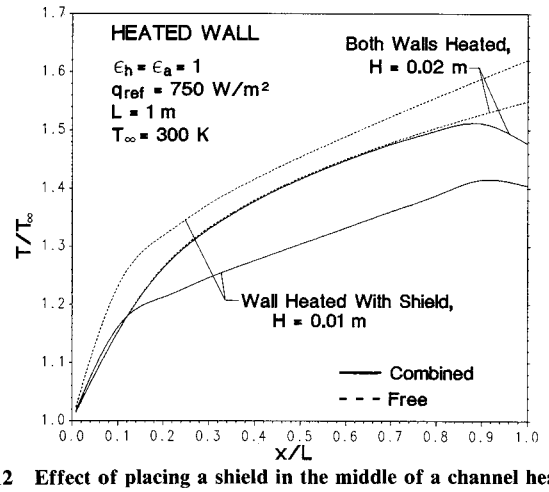


Fig. 12 Effect of placing a shield in the middle of a channel heated uniformly on both walls.

the latter part of the channel. For the adiabatic wall in Fig. 9b, the presence of radiation seems to reduce the significance of the channel width on the adiabatic wall temperature.

The effects of the emissivities on the two wall temperatures are illustrated in Figs. 10a and 10b. As expected, the effect of radiation on both wall temperatures diminishes with decreasing emissivities. When the emissivities of the heated and adiabatic walls are interchanged, the temperature of either wall is only affected near the exit of the channel, due to the radiative losses to the cooler surroundings.

In Figs. 11a and 11b, the inlet temperature effects on the heated and adiabatic wall temperatures are depicted, respectively. As can be observed from the two figures, the relative shift in the wall temperatures due to the presence of radiation seems to be insensitive to the inlet air temperature for the specified conditions.

Finally, Fig. 12 exhibits the effect of placing a shield in the middle of a channel heated uniformly at the same rate on both sides. As attested from the figure, when there is no shield in the channel that is heated uniformly on both sides ($H = 0.02$ m), the radiation effect is negated by the symmetry in the channel, and it only manifests its presence near the exit of the channel due to the radiative losses to the surroundings. When a shield is placed in the middle of the same uniformly heated channel, making the channel width in each half $H = 0.01$ m, the net radiation exchange between each of the heated walls and the shield induces the reduction in the heated wall temperature shown in Fig. 12.

## Summary

An assessment of the effects of the uniform rate of heat transfer, channel length, channel width, inlet air temperature, and surface emissivities on the radiation-associated respective reduction of the heated wall temperature and elevation of the adiabatic wall temperature is presented. The redistribution of the supplied energy of the heated wall due to radiation tends to bring the temperatures of the heated and adiabatic walls closer together. For the specified conditions, the magnitude of the net radiative transfer remains approximately the same in the majority of the channel, except near the inlet and exit, where radiation with the surroundings can be quite important. Considerable increases in the average velocity over those for pure free convection may occur because of radiation. Finally, significant decreases in the wall temperatures of a symmetrically heated channel may be achieved by placing a shield in the middle of the channel to activate the otherwise dormant radiation mode.

## References

[1]Keshock, E. G and Siegel, R. "Combined Radiation and Convection in an Asymmetrically Heated Parallel Plate Flow Channel," *Transactions of the American Society of Mechanical Engineers, Series C, Journal of Heat Transfer,* Vol. 86, Aug. 1964, pp. 341-350.

[2]Liu, S. T. and Thorsen, R. S., "Combined Forced Convection and Radiation Heat Transfer in Asymmetrically Heated Parallel Plates," *Proceedings of the Heat Transfer and Fluid Mechanics Institute,* Stanford Univ. Press, Palo Alto, CA, 1970, pp. 32-44.

[3]Sparrow, E. M., Shah, S., and Prakash, C., "Natural Convection in a Vertical Channel: I. Interacting Convection and Radiation. II. The Vertical Plate With and Without Shrouding," *Numerical Heat Transfer,* Vol. 3, July-Sept. 1980, pp. 297-314.

[4]Carpenter, J. R., Briggs, D. G., and Sernas, V., "Combined Radiation and Developing Laminar Free Convection Between Vertical Flat Plates with Asymmetric Heating," *Journal of Heat Transfer,* Vol. 98, Feb. 1976, pp. 95-100.

[5]Patankar, S. V. and Spalding, D. B., "A Calculation Procedure for Heat, Mass, and Momentum Transfer in Three-Dimensional Parabolic Flows," *International Journal of Heat and Mass Transfer,* Vol. 15, Oct. 1972, pp. 1787-1806.

[6]Patankar, S. V., *Numerical Heat Transfer and Fluid Flow,* Hemisphere, Washington, DC, 1980.

[7]Raithby, G. D. and Schneider, G. E., "Numerical Solution of Problems in Incompressible Fluid Flow: Treatment of the Velocity-Pressure Coupling," *Numerical Heat Transfer,* Vol. 2, Oct.-Dec. 1979, pp. 417-440.

[8]Aung, W., Fletcher, L. S., and Sernas, V., "Developing Laminar Free Convection Between Vertical Flat Plates with Asymmetric Heating," *International Journal of Heat and Mass Transfer,* Vol. 15, Nov. 1972, pp. 2293-2308.

[9]Wirtz, R. A. and Stutzman, R. J., "Experiments on Free Convection Between Vertical Plates with Symmetric Heating," *Journal of Heat Transfer,* Vol. 104, Aug. 1982, pp. 501-507.